



# Robotic on-site adaptive thin-layer printing: Challenges and workflow for design and fabrication of bespoke cementitious plasterwork at full architectural scale

Selen Ercan Jenny<sup>1</sup> · Daniela Mitterberger<sup>1</sup> · Ena Lloret-Fritschi<sup>1</sup> · Lauren Vasey<sup>1</sup> · Elliott Sounigo<sup>1</sup> · Ping-Hsun Tsai<sup>1</sup> · Petrus Aeijmelaeus-Lindström<sup>1</sup> · David Jenny<sup>1</sup> · Fabio Gramazio<sup>1</sup> · Matthias Kohler<sup>1</sup>

Received: 30 March 2022 / Accepted: 12 July 2022 / Published online: 1 September 2022

© The Author(s) 2022

## Abstract

This paper describes the 1:1 scale application of Robotic Plaster Spraying (*RPS*), a novel, adaptive thin-layer printing technique, using cementitious base coat plaster, realized in a construction setting. In this technique, the print layers are vertical unlike most *3DCP* processes. The goal is to explore the applicability and scalability of this spray-based printing technique. In this study, *RPS* is combined with an augmented interactive design setup, the Interactive Robotic Plastering (*IRoP*), which allows users to design directly on the construction site, taking the building structure, as-built state of the on-going fabrication and the material behavior into consideration. The experimental setup is an on-site robotic system that consists of a robotic arm mounted on a semi-mobile vertical axis with an integrated, automated pumping and adaptive spraying setup that is equipped with a depth camera. The user interaction is enabled by a controller-based interaction system, interactive design tools, and an augmented reality interface. The paper presents the challenges and the workflow that is needed to work with a complex material system on-site to produce bespoke plasterwork. The workflow includes an interactive design procedure, localization on-site, process control and a data collection method that enables predicting the behavior of complex-to-simulate cementitious material. The results demonstrate the applicability and scalability of the adaptive thin-layer printing technique and address the challenges, such as maintaining material continuity and working with unpredictable material behavior during the fabrication process.

**Keywords** Spray-based printing · Prediction models for complex materials · Augmented interactive design · On-site mobile fabrication · Bespoke cementitious plasterwork

## Introduction

Plasterwork used on interior walls and ceilings, as well as on facades, can play both functional and ornamental roles such as protecting the building structure or improving acoustic performance, thermal properties, and visual qualities [1]. Conventional manual plastering is a craft that requires a certain skill set, involving the application of centimeter-thick layers of plaster that are either troweled to a smooth, flat surface or shaping of the wet material with custom made tools such as

a running mold, exploring the potentials of the material for producing architectural articulations [2]. Similarly, in the field of digital fabrication, profiling tools have been combined with agile robotic arms to explore subtractive or hybrid fabrication techniques, which combine additive and subtractive processes [3, 4]. Robotic Plaster Spraying (*RPS*) introduces an adaptive, thin-layer, spray-based printing technique aiming to explore new, bespoke design possibilities through a digital process that is based on additive manufacturing. Ultimately, the goal is to use a fully mobile fabrication process that can perform continuous, non-horizontal printing on-site. *RPS* involves spraying of multiple, millimeter-thin layers of plaster onto a building structure, a process which enables the incremental build-up of 2D- and 3D- formations, without the use of additional formwork or support structures, producing minimal waste. It uses process parameters - such as distance, angle, and speed of the robotic arm - to control the material formation. In other words,

✉ Selen Ercan Jenny  
ercan@arch.ethz.ch

<sup>1</sup> Institute of Technology in Architecture (ITA), Gramazio Kohler Research, ETH, Stefano-Francini-Platz 1, CH-8093 Zurich, Switzerland

the malleability of the wet material combined with the digitally controlled, pneumatic spraying method acts as the dynamic formwork for the resulting surface geometry or pattern. To explore the possible formations with this spray-based printing process, we have developed a workflow in which we collect data from the physical results. The data is used to model the effect of the fabrication parameters in line with the material, both with linear and nonlinear functional relations. These enable us to predict the complex-to-simulate material behavior, which are further described in [5].

Materials, such as cementitious plaster, still require human interaction, as ambient conditions (i.e. differences in temperature or moisture, variation of raw materials, inconsistencies in mixing or pumping) can result in changes in the rheological properties resulting in failures during production such as i.e. clogging, leading to unpredictable results on-site. With this goal, *RPS* was combined with an interactive design system, coined with the name, Interactive Robotic Plastering, *IRoP* [6]. *IRoP* utilizes on-site, interactive design tools and a projection-based augmented reality interface for *RPS*, addressing diverse users with limited robotic and computational knowledge. The goal of this study is to apply the adaptive thin-layer printing technique in 1:1 scale, onto an existing building structure, resulting in an articulated, cementitious plasterwork. It was designed on-site, in parallel to on-going fabrication, taking the existing building structure and the as-built state of the design into consideration - to make the necessary adaptations interactively, and on the fly. It was fabricated with an on-site robotic system that enables adaptive fabrication while introducing challenges such as material continuity on the corners and edges of the building structure and the impact of segmentation on the material. The application was part of a design and building project within the Master of Advanced Studies ETH in Architecture and Digital Fabrication programme, and executed in Rümlang, Switzerland (Fig. 1). This paper focuses on the challenges and the workflow of the 1:1 scale application.

As shown in Fig. 2, the on-site design and fabrication workflow comprises: (1) Interactive computational model and design procedure [6] that is followed by (2) Localization (of the robotic system) on-site [7], which provides the necessary positioning data for the (3) Process control for adaptive thin-layer printing [5, 8], which is used in every iteration of the fabrication loop that comprises (4) Application to building structure, enabling (5) Data collection and (6) Prediction and visualization informing the design process prior to fabrication [5].

## Relevant work

Since the 1990s, researchers have worked to automate the plastering process, applying plaster with a robotic arm with multiple degrees of freedom (DoF) that is equipped with

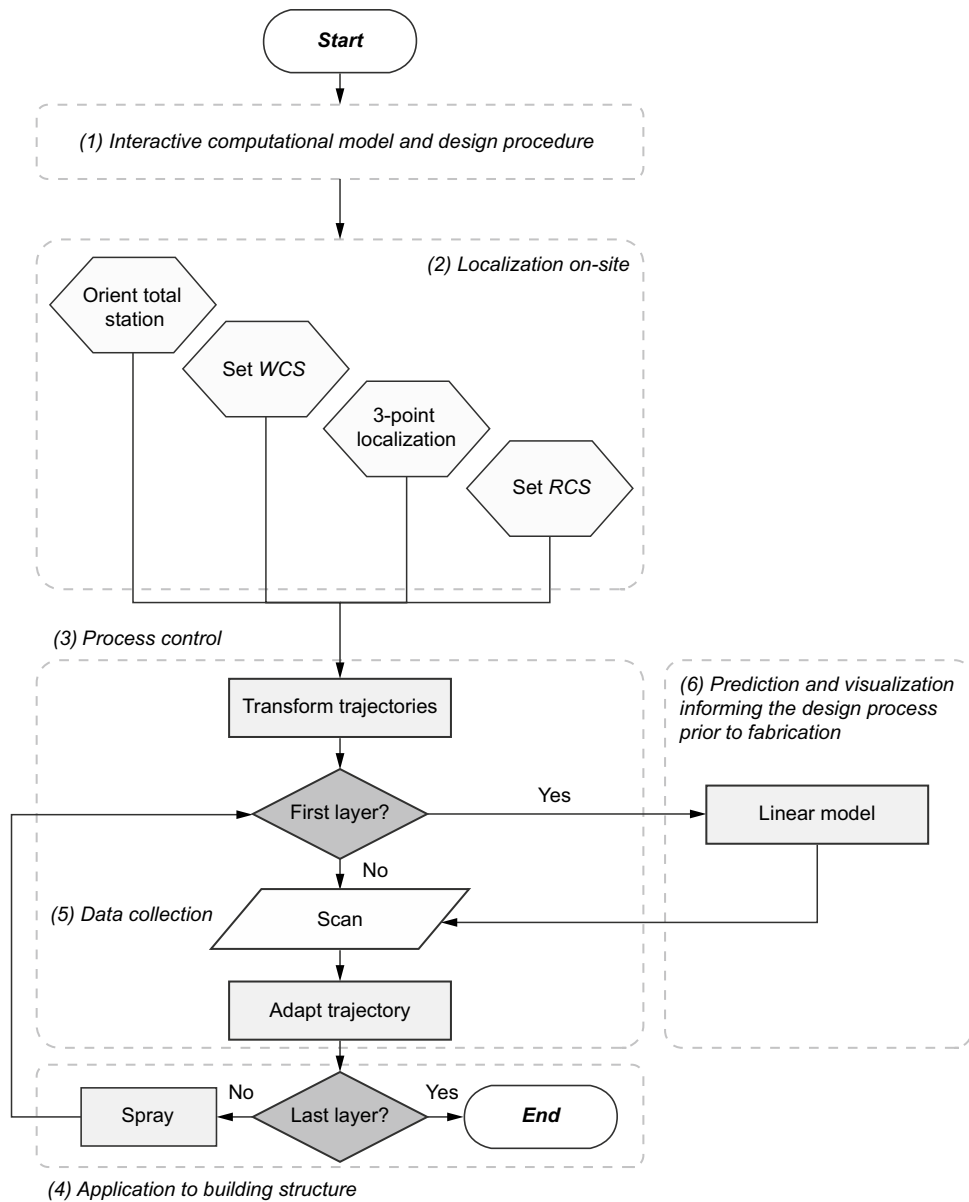


**Fig. 1** 1:1 scale application of Robotic Plaster Spraying (*RPS*) in a real construction setting, as part of a design and building project within the Master of Advanced Studies ETH in Architecture and Digital Fabrication programme

tools that can spray, apply or level plaster [9–12]. While standardized plasterwork can be automated with such approaches, these processes neglect to take full advantage of the three-dimensionality of the material and its potential for architectural articulations. Such approaches seek to imitate the steps of producing simplified plasterwork for standardized, flat surfaces, but they fail to use the digitally controlled fabrication process to explore the inherent material properties that enable 3D-formations [13, 14]. To explore these properties with complex-to-simulate (cementitious) materials in digitally controlled processes, the design workflow needs to be informed and take material constraints into account. This requires tailored sensing solutions, which are integrated into the fabrication process. Like this, fabrication parameters can be related to the sprayed surface geometries or patterns allowing for an intuitive design process - that can predict the complex-to-simulate material behavior, prior to fabrication.

Within the fields of sensing systems and digital fabrication, methods exist that can address surface finish classification or determine the roughness of surfaces produced with cementitious materials, also specifically with plaster [15–17]. Such methods use sensing for geometric inspection and quality control, but they do not yet attempt to relate the features of the surface topographies to fabrication parameters. A similar gap exists in the spray-based 3D printing research with cementitious materials. Examples such as Shotcrete 3D Printing (*SC3DP*) [18, 19], Robotic AeroCrete [20, 21] or similar research projects on robotic concrete spraying [22] use sensing for fabrication control (during or post- production) but not yet for informing the design process. The Spray-Based 3D Concrete Printing (*S-3DCP*) research at NTU [23] starts to investigate the effect of process parameters on material distribution in a spray-based 3D

**Fig. 2** On-site design and fabrication workflow



concrete printing process. *S-3DCP* uses an analytical model to understand material behavior and guide the selection of suitable parameters, such as the spray width and thickness for the quantitative deposition of the material on a target surface. Although *S-3DCP* explores material behavior, it has not yet included this information in the design process. As such, it lacks the means to design with the physical properties and constraints of such complex, malleable materials, targeting diverse surface qualities and using a software workflow that serves to inform the design and fabrication process on-site. In the presented study, we explored such a material informed design and fabrication process through an on-site workflow. In addition to predicting the sprayed results prior to fabrication, the users could design interactively on-site, taking the building structure, as-built state

of the on-going fabrication and the material behavior into consideration (Fig. 3).

## Design and fabrication concept

This section describes the on-site design and fabrication workflow as shown in Fig. 2. Firstly, the user follows the interactive design procedure (Section 3.1). As a next step, the 3-point localization method is executed (Section 3.2.1). After each spraying layer, the target surface is scanned to adapt the robot trajectories - the spray paths (Section 3.2.2) - and to store the resulting geometry and pattern in line with the fabrication parameters (Section 3.2.3). If it is the very first layer, before starting the adaptive thin-layer printing on

**Fig. 3** Adaptive thin-layer printing on-site, in process, while the users can design interactively utilizing the projection-based augmented reality interface, taking the as-built state of the on-going fabrication, building structure and the material behavior into consideration



the walls of the room, the physical outcome is predicted and visualized using the linear model, to inform the design process (Section 3.2.3). Each step is described in detail below.

### Interactive computational model and design procedure

The interactive computational model and design procedure of *IRoP* that is presented in [6], enables users to design, preview and record a set of spray paths (robot trajectories) on-site - projected on to the walls of the room<sup>1</sup> - in real-time (step 1, Fig. 2). To ensure tacit user interaction, the system records hand movements with a controller-based interaction tracking system. This system includes a customized *HTC VIVE* setup with two base stations (Fig. 4, “B”) and one controller (Fig. 4, “C”)<sup>2</sup>. The tracking of the controller’s position is registered in three dimensions and in relation to the building structure. For this purpose, the system uses a stored digital twin of the room to calculate the controller’s position in relation to a target surface, such as the wall of the

room. Besides tracking the user input, the interactive computational model of *IRoP* remaps the analogue human input to robotic output, translating human gestures into fabrication parameters (Table 1). It translates the user’s hand position in space,  $P$ , and hand distance to the target surface (the wall),  $D$ , to the end-effector distance to the target surface,  $E_d$ . End-effector pitch and yaw angles are programmed by the user and not influenced by hand gestures. Gesture velocity,  $V_h$ , is remapped and scaled to the velocity of the trajectory,  $V$ . Furthermore, hand distance to the target surface,  $D$ , influences  $L_n$ , the number of layers that is needed to be sprayed to achieve a specific geometry or pattern<sup>3</sup>. The system directly generates robot trajectories and the fabrication parameters - by the user adjusting and applying different stylistic filters<sup>4</sup> to the recorded human input, using the computational model - which define the spray outcome.

### On-site fabrication process

As shown in Fig. 4, the overall robotic fabrication setup for process control comprises a spraying tool that consists of (K) a pneumatic *POWER-SPRAYS LW Facing Coat Spray*

<sup>1</sup> Currently the system is tested on planar walls as a first step, but the technology can be extended to non-planar surfaces with minor adaptations.

<sup>2</sup> To receive data from the tracking system, we used the Robot Operating System (*ROS*) - <https://www.ros.org/>, a scalable, near real-time communication system. Using the publish-and-subscribe architecture of *ROS* in combination with the *rosbridge* package [24] we were able to send the user input in form of 6-DoF position and orientation of the controller to the interactive computational model.

<sup>3</sup>  $N_d$  is kept constant at 9.5 mm for this application.

<sup>4</sup> As presented in [6], stylistic filters are methods within the interactive computational model, which allow the user to define how to utilize hand gestures for robotic actions. The system can be used to develop custom filters. These custom filters allow designers to quickly develop diverse architectural articulations with *RPS*.

**Table 1** Table showing the fabrication parameters of *RPS* and the translated hand gestures

Abbreviation	Explanation	Unit
$P, D \rightarrow E_d$	Hand position in space, Hand distance to target surface → End-effector distance to the target surface	mm
$E_{a1}$	End-effector pitch angle in reference to the target surface	°
$E_{a2}$	End-effector yaw angle in reference to the target surface	°
$V_h \rightarrow V$	Gesture velocity → Velocity of the trajectory	m/s
$D \rightarrow L_n$	Hand distance to target surface → Layer number	—
$N_d$	Nozzle diameter of the pneumatic (plastering) spray gun	mm

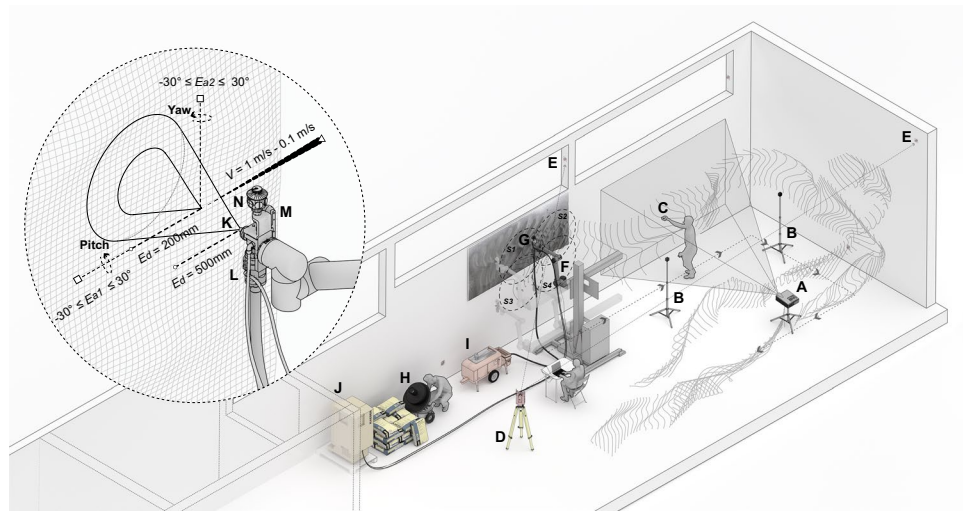


**Fig. 4** The interactive design procedure includes (A) a projection-based augmented reality system where the recording of spray paths is enabled by a customized *HTC VIVE* with (B) two base stations and (C) one controller. For the global localization of the semi-mobile robotic system in the room, (D) a *Hilti POS 150* total station is used for defining a world coordinate system (WCS) by measuring minimum two of the 10 pre-recorded and fixed reference points on

the walls of the room (E). The overall robotic fabrication setup comprises (F) a 6-DoF manipulator - a collaborative robotic arm - *UR10* mounted on a 2-DoF external axis tower by *Güdel* (that is moved manually on-site), (G) a spraying tool, (H) a *Collomatic Collomix XM2* mixer, (I) a modified *PFT Swing L* pump, and (J) a *Kaeser SXC* series compressed air system

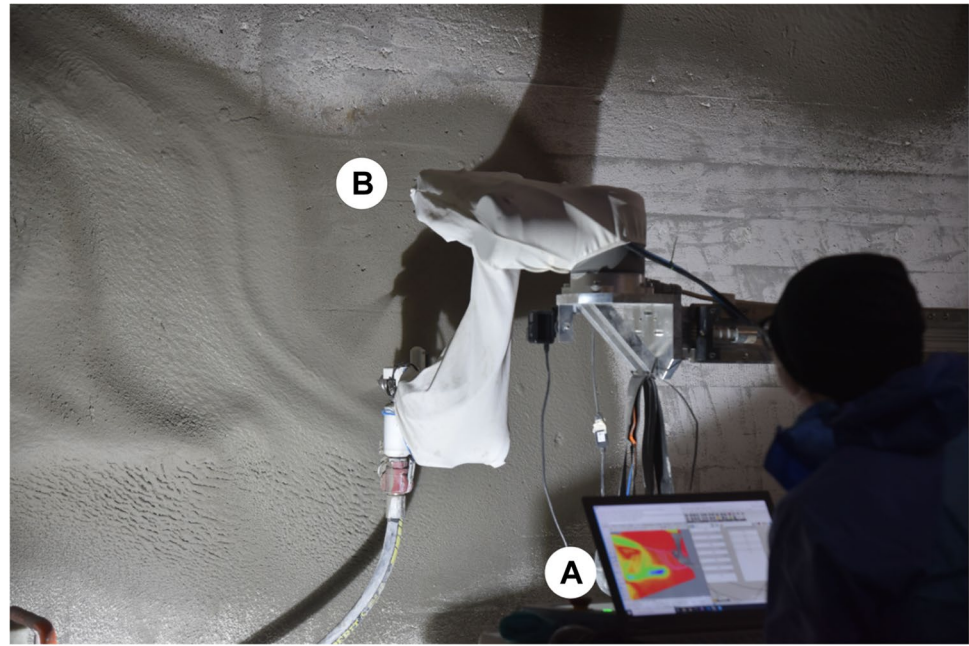
*Gun*, (L) a *HO-Matic* pinch valve series 00, (M) an *Intel RealSense Depth Camera D455*. The *POWER-SPRAYS LW Facing Coat Spray Gun* contains a 9.5 mm, tapered, removable nozzle at the tip and an air inlet to allow for spraying of a wide range of cementitious or other pumpable materials. The start and the stop of spraying are digitally controlled. The time delays in the material flow is regulated by the *HO-Matic* pinch valve<sup>5</sup>. As shown in Fig. 4, the spraying tool is mounted on a (F) a 6-DoF manipulator - a collaborative robotic arm - *UR10*, which is mounted on a custom, manually driven, 2-DoF external axis tower by *Güdel*. The material used for fabricating the articulated plasterwork is a dry-mix, base coat lime-cement plaster (*Weber IP 18 Turbo*). It is mixed externally in batches of 25 kg to 30 kg, with

(H) a *Collomatic Collomix XM2* mixer on-site. It is fed into the pneumatic spray gun by (I) a modified *PFT Swing L* (conveying) pump that is driven by the *UR10* robot controller. To activate the pneumatic spray gun, (J) a *Kaeser SXC* series compressed air system is used. The air pressure used for the pneumatic spray gun is kept constant at ~50 psi. The modifications to the pump include the integration of a custom control board and a frequency converter that allow for interfacing with the *UR10* robot controller, which are needed for reducing the pumping speed to a range of ~0.5 l/min to ~5 l/min. They also enable the digital control of the pump start, stop and running speed, which is kept constant at ~1.7 l/min. With a constant pumping speed, the feed rate of the material is set by the robotic arm (through the velocity of the trajectory,  $V$ ).

The custom, 2-DoF external axis tower extends the work envelope of the robotic arm by 2 m horizontally and 3 m vertically. The setup is moved manually on-site, to

<sup>5</sup> Through using a pinch-valve, ~5 s decrease in time delay for the start and stop of the material flow is observed in the experiments.

**Fig. 5** (A) Acquiring the geometry of the target surface for adapting the non-horizontal spray paths to (B) the actual (as-built) state of the articulated surface building-up on the building structure



various positions using a pallet jack and is stabilized by leveling its four adjustable feet. Overall, this semi-mobile, extendable robotic system provides a total reachability of ~4 m in height and offers an adaptive, on-site fabrication process when combined with the localization strategy described below. The ultimate goal of *RPS* is to employ a fully mobile machine, however the use of this semi-mobile robotic system for adaptive thin-layer printing on a real building structure played an important role in addressing the challenges of the on-site fabrication of bespoke plasterwork and the continuity of the material - the continuous spraying<sup>6</sup>. As such, developing different segmentation strategies became a key challenge for the design, which reflected the necessary break in the spray paths - *the segments* - as a result of relocating the robotic system to various positions in the room.

#### Localization on-site

For the global localization of the robotic system in the room (step 2, Fig. 2), a *Hilti POS 150* total station<sup>7</sup> was used (Fig. 4, “D”) to apply the 3-point localization method described in [7]. The first step in localizing the

robotic system is to orient the total station for defining a world coordinate system (*WCS*) by measuring minimum two of the 10 pre-recorded and fixed reference points on the walls of the room (Fig. 4, “E”). After this, the position of the 360° reflector prism mounted on the spraying tool (on the *UR10*, Fig. 4, “N”) is measured and recorded for three different points in space, which correspond to three different configurations of the robotic arm. The first point sets the origin of the robot coordinate system (*RCS*); the second point sets the *X-Axis* of the *RCS*; and the third point sets the *Y-Axis* of the *RCS*, defining a 3-point localization method. Following, in the digital building model of the room, the origin of the *RCS* stays unchanged, and the rest of the geometries, such as walls and spray paths are transformed. In this way, the robot trajectories are transformed from *WCS* to *RCS*. After the robotic system is relocated to the new position in the room and the global transformation (the position in space and in relation to the last position) is calculated, each axis transformation is computed locally to ensure that the spray paths on the walls remain within the reachability of the *UR10* on the external axis tower.

#### Process control for adaptive thin-layer printing

To acquire the geometry (of the actual state of the target surface, Fig. 5), an *Intel RealSense Depth Camera D455*, mounted on the spraying tool is used. For this, a target spraying surface is reconstructed and visualized in the 3D

<sup>6</sup> Additional challenges included keeping the room temperature above 0°C to assure good mixing quality and to minimize the variation in different batches.

<sup>7</sup> The *Hilti POS 150* offers a distance precision of  $2\text{mm} \pm 2\text{ppm}$ , an angle precision of 5 family” (~0.00139°) and a measurement range of ~1000 m.

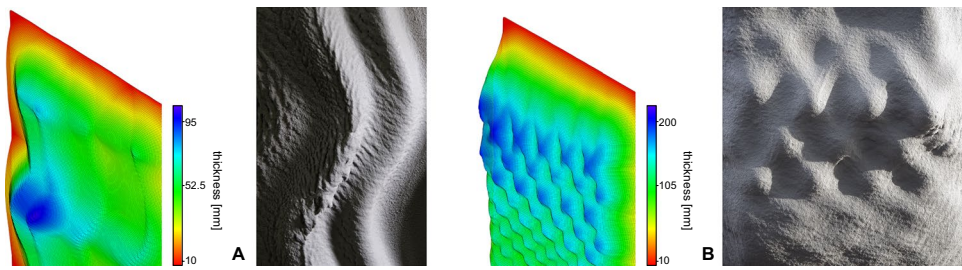


**Fig. 6** Predictions with the linear model and the respective physical results in (A) exploration with  $E_{a2}$ , leading to variations in surface roughness and granularity. From left to right,  $E_{a2}$  starts with a value of  $30^\circ$  and ends with  $0^\circ$ . Result of 40 layers, with velocity of spraying,  $V = 0.6 \text{ m/s}$ , and with an average distance of spraying,  $E_d$ , of 350 mm. Maximum thickness (overhang):  $\sim 95 \text{ mm}$ . (B) Exploration

with  $V$  and  $L_n$ , leading to a volumetric build-up of the material on the building structure. Result of 18 layers, with velocity of spraying,  $V$ , varying between 0.1 m/s and 1 m/s and distance of spraying,  $E_d$ , varying between 300 mm and 500 mm. Overall volume:  $\sim 0.03 \text{ m}^3$  with maximum thickness (overhang):  $\sim 200 \text{ mm}$  ( $\sim 210 \text{ kg}$  of material). Fabrication time:  $\sim 2.5$  hours

modeling and visual programming environment *Rhino Grasshopper*<sup>8</sup>. As shown in step 3 in Fig. 2, the robot trajectory (spray path) is adapted to the spraying distance ( $E_d$ ) set by the user (Table 1), by projecting it onto the actual state of the target surface, with the methods implemented in [5, 8]. While keeping  $V$  unchanged,  $E_d$  regulates the layer thickness, and assures to avoid collisions of the robotic arm with the as-built state of the target spraying surface. In addition to adapting the non-horizontal spray paths to the actual (as-built) state of the articulated surface that is building-up, scanning also serves to collect data<sup>9</sup> - which is described below.

#### Application to building structure, data collection, prediction and visualization informing the design process prior to fabrication

The dimensions of the building structure are 5.8 m by 15.8 m with a height of 5 m, resulting in a wall surface of  $\sim 200 \text{ m}^2$ . To spray the material on the walls, the robotic system is moved to 11 different positions in the room. Each position includes up to 4 segments of spray paths (Fig. 4, S1-S4).

After each segment is sprayed (step 4, Fig. 2), the data collection step is executed and the as-built state of the articulated surface segment is stored as described below.

In the method presented in [5], the sprayed result is represented by a transformed mesh and the transformation of the vertices is computed for two consecutive states of the surface geometry (consecutive layers). By computing this transformation after each layer, the overall thickness or the pattern (and the fabrication parameters used) - is tracked vertex-by-vertex (step 5, Fig. 2). For the initial tests and the 1:1 scale application on-site, the linear model that is presented in [5] is used as a base (Figs. 6 and 9), to predict and visualize the (3D) spray outcome of the recorded spray paths (step 6, Fig. 2). This model establishes the relationship between the input (i.e.  $E_d$ ,  $V$ ,  $L_n$ ) and the output (sprayed thickness), through mapping the minimum and the maximum input values to the output (i.e. an  $E_d$  range of 300 mm to 500 mm is mapped to a layer thickness of 6 mm to 3 mm), thus providing an approximate representation of the possible outcome and an empirical understanding of the fabrication parameters and their effects.

## Results

### Initial experiments

Prior to the application on-site, initial experiments were conducted to explore the maximum thickness that can be built as an overhang on a vertical surface, as well as the effect of distance, angle and velocity of spraying. For the exploring the maximum distance, the velocity of the trajectory,  $V$ , varied in a range from 0.1 m/s to 1 m/s. In Fig. 6, “B” illustrates the resulting 19 layers, fabricated in  $\sim 2.5$  hours, with  $V$  varying between 0.1 m/s and 1 m/s, with an overall volume of  $\sim 0.03 \text{ m}^3$  and with a maximum thickness (overhang) of  $\sim 200 \text{ mm}$  ( $\sim 210 \text{ kg}$  of material). As hand distance to target surface,  $D$ ,

<sup>8</sup> <https://www.grasshopper3d.com/> Additionally, to simulate the robot trajectories before execution, the kinematic model of the UR10 is visualized in the same environment, using the COMPAS FAB ([https://github.com/compas-dev/compas\\_fab](https://github.com/compas-dev/compas_fab)) package of the open-source, Python-based computational framework COMPAS (<https://github.com/compas-dev/compas>).

<sup>9</sup> Acquiring the target surface and the adaptation of spray paths are facilitated with software modules built within the COMPAS framework and are visualized in *Rhino Grasshopper*, with dependencies on the 3D data processing library Open3D (<https://github.com/isl-org/Open3D>) and the pyrealsense2 (<https://github.com/IntelRealSense/librealsense/tree/master/wrappers/python>) of Intel RealSense SDK 2.0. Scanning and streaming the data to *Rhino Grasshopper* takes  $\sim 120 \text{ s/m}^2$ . Intel RealSense Depth Camera D455 offers a depth accuracy of  $< 2\%$  at 4 m.

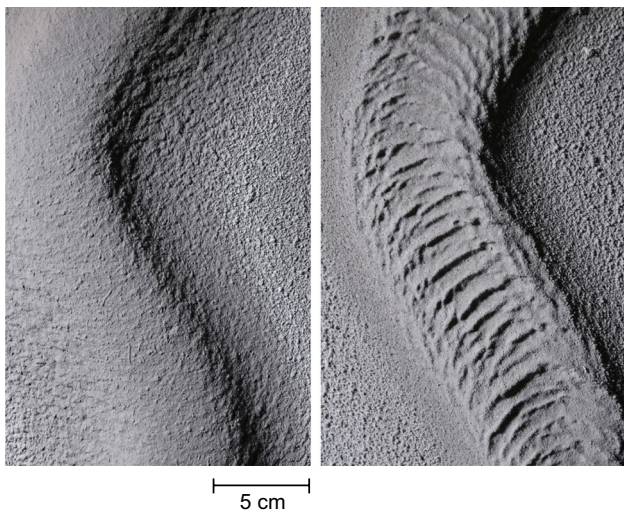


**Fig. 7** Results from the exploration with the end-effector distance to the target surface,  $E_d$  (distance of spraying) leading to a smooth surface quality (on the left, with  $E_d > 300$  mm) and a “carving effect” on the material (on the right, with  $E_d < 300$  mm). In both tests, velocity of spraying,  $V = 0.8$  m/s, the end-effector pitch and yaw angles in reference to the target surface,  $E_{a1}$  and  $E_{a2}$  are kept constant at  $0^\circ$ .  $N_d = 9.5$  mm, pumping speed and the air pressure used for the pneumatic spray gun are also kept constant at  $\sim 1.7$  l/min and at  $\sim 50$  psi, respectively

influenced the number of layers that is needed to be sprayed to achieve a specific geometry or pattern,  $L_n$ , and gesture velocity,  $V_h$ , was remapped and scaled to the velocity of the trajectory,  $V$ , linearly, the user could choose to use slower hand movements, in relation to the target surface, for having predominantly larger overhangs at chosen areas.

In the tests exploring the distance of spraying, hand distance to target surface,  $D$  (within a range of 5 mm to 1000 mm), was related linearly to end-effector distance to the target surface,  $E_d$ . Starting from smooth, and then amplifying the effect of displacing certain portions of the wet plaster with the air pressure used for the pneumatic spray gun, these tests resulted in a “carving effect” when the user’s hand was closer to the target surface (Fig. 7).

Explorations with the end-effector pitch angle in reference to the target surface,  $E_{a1}$ , showed that higher values led to smoother transitions from the articulated plasterwork to the target surface (and for application on-site, to the walls, along the height of the room). Explorations with end-effector yaw angle in reference to the target surface,  $E_{a2}$ , showed that higher values (within the given range) led to more variations in surface roughness as shown in Fig. 6, “A”. From left to right,  $E_{a2}$  starts with a value of  $30^\circ$  and ends with  $0^\circ$ , where the result of 40 layers can be seen with  $V = 0.6$  m/s, and with an average  $E_d$  of 350 mm. As the angle of spraying also enlarged the work envelope of the robotic arm by enlarging the spray cone with the rotation of the end-effector, this

advantage was utilized on-site when the robotic arm was close to its reachability limits (the borders of the segments): Layer thickness could vary in a gradient (of  $\sim 6$  mm to  $\sim 3$  mm) with changing end-effector pitch and yaw angles, thus they were programmed by the user to blend the material to the wall, for creating smooth connections over larger spans.

### Application on-site

The application on-site started with the design of the spray paths by the users of the system, that comprised of recording and applying different stylistic filters to the recorded input. Within the interactive design procedure, an already printed path was not revisited however; the user could design the future paths interactively on-site taking the building structure and the as-built state of the on-going fabrication into consideration. Like this, the user could have a decision making process on-site that impacts the overall design of the continuous, articulated plasterwork. This was followed by the localization of the robotic system on-site to initiate process control for consecutive spraying sessions. In addition to adapting the spray paths to the actual state of the target surface, scanning also served acquiring the geometry of the articulated surface building-up on the building structure, in line with the fabrication parameters (data collection). Before each spraying session, the (3D) spray outcome of the spray paths were visualized using the linear prediction model (Fig. 9).

The articulated plasterwork was planned as a permanent installation, which was not meant to test the performative aspects of plastering, such as thermal properties or acoustic performance, but rather aimed to evaluate the applicability and scalability of the methods in a real construction setting. It was executed in  $\sim 10$  days with  $\sim 3400$  kg of lime-cement plaster and in  $\sim 52$  hours of spraying. The overall volume of the installation is  $\sim 2.7$   $m^3$  with a maximum overhang of  $\sim 165$  mm. The average number of layers sprayed,  $L_n$ , is  $\sim 25$ .

### Impact of segmentation on the material

Tests “A” and “B” shown in Fig. 8, illustrate two segmentation strategies in the vertical direction - along the height of the room. Both aim for a blending effect to maintain the continuity of the articulated installation without obvious interruptions - cold joints - between the segments. Figure 8 “A”, shows the first test - vertically segmented and overlapping spray paths (numbered 1-14 in the diagram). The result of the spray paths 6-10 or 11-14, resulted in a clear indication of the joints. Figure 8 “B”, shows the second test - vertically segmented and non-overlapping spray paths with varying  $E_d$  (paths 1-2), or with varying  $V$  (paths 3-4). As this strategy also did not result in a continuous material articulation, for the overall application in the room, we decided to combine

**Fig. 8** Tests (A) and (B) on segmentation, addressing the challenge of maintaining the material continuity in the vertical direction. (C) Segmentation of the (vertically continuous) spray paths in the horizontal direction. (D) A seamless, smooth corner detail with a volumetric build-up

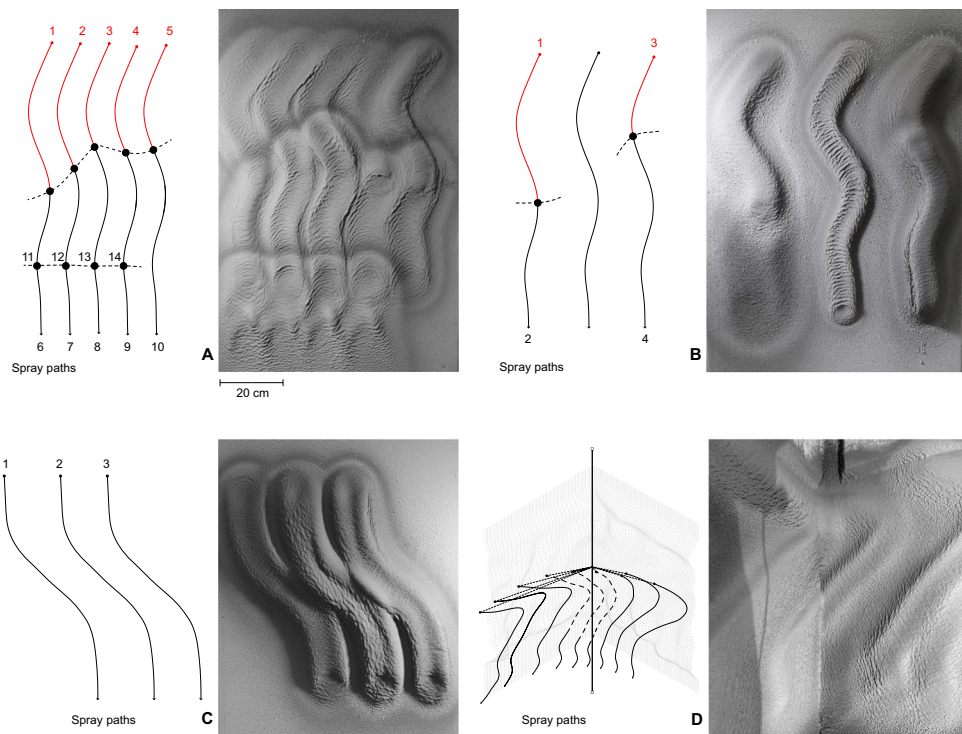
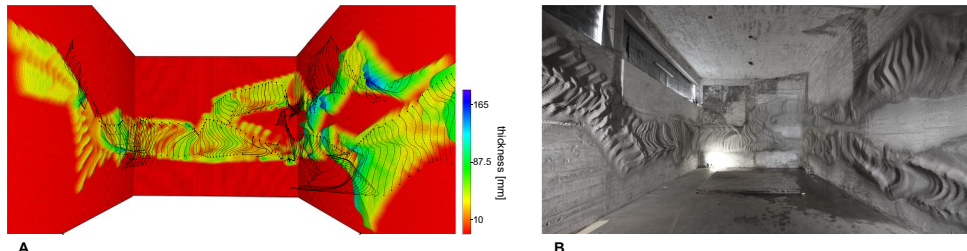


**Fig. 9** (A) Predicted result from the linear model (for all segments, merged). (B) Overall physical result, which combined the segmentation of the (vertically continuous) spray paths in the horizontal direction - along the width of the room - with a “branching” strategy



the segmentation of the (vertically continuous) spray paths in the horizontal direction - along the width of the room (Fig. 8, “C”) with a “branching” strategy (Fig. 9). This strategy allowed a height of  $\sim 3.85$  m to be reached, while still maintaining the continuity of the installation in the overall room.

#### Continuity on the corners and edges

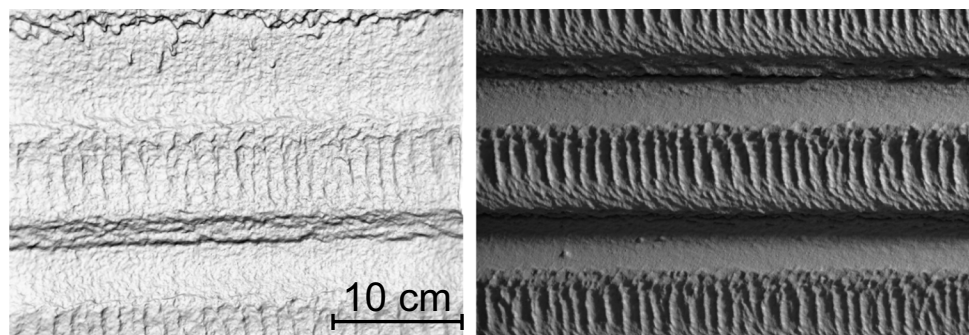
The main challenge of details for corners or ceiling and floor edges is the deposition of equally distributed material, in order to ensure a smooth transition. In the presented application, to achieve this on the corners of the room, the velocity of the trajectory (spray path),  $V$ , which defines the feed rate of the material, was lowered where the distance of the spray path to the intersection of two target surfaces was shorter (Fig. 8, “D”, dashed lines). This approach resulted in an increased feed rate of the material in the areas where the spray path was closer to the corner, ensuring a seamless,

smooth corner detail with a volumetric build-up and the continuity of the bespoke plasterwork.

#### Conclusion

**Interactive computational model and design procedure** The process presented in this paper explores a creative usage of digital fabrication that includes design adaptations on the fly and a bespoke fabrication process, with an on-site robotic system. It provides an understanding of a human-in-the-loop workflow in specific to a complex material process. It explores and demonstrates the potential for integrating the tacit knowledge of humans to on-site fabrication. Based on this exploration, reacting to unpredictable results on-site and taking decisions on the fly while designing in parallel to ongoing fabrication - in respect to the *as-built* - can be further tested. Like this, we can address additional challenges and

**Fig. 10** Outlook on scanning with a *LUCID Helios* time-of-flight 3D camera, to allow for data collection on the quality of the sprayed result (on the right) with a higher resolution mesh (on the left). Result of 15 layers, with velocity of spraying,  $V = 0.55 \text{ m/s}$  and distance of spraying,  $E_d = 200 \text{ mm}$ . Maximum thickness (overhang):  $\sim 50 \text{ mm}$



assess the feasibility of the approach for other applications on a construction site.

#### On-site localization of the robotic system and process control

The setup presented in this paper demonstrates both the potential and the challenges of on-site fabrication. The fully-mobile robotic platform that is being currently developed to be implemented in future research, should further expand the possibilities for this technology. A constant material-feed combined with a fully mobile robotic platform - with synchronized arm and base movements [25] - will allow *RPS* to be applied as a continuous mobile 3D printing process on-site [8, 26], easing the challenge of segmentation and to avoid the formation of cold joints. Still, transitioning to the existing building structure - i.e. from floor to wall, wall to ceiling, as well as controlling tolerances according to specific situations (such as corners or deviations in the building structure) will challenge the process applicability. However, from a design point of view, both semi- and fully mobile approaches offer interesting ways to define interfaces with existing structures or between segments, rather than treating them as discrete patches on a wall, as it becomes possible to blend surfaces through process control. Many effects can be further developed, such as creating smooth transitions and enhancing connection details like accentuated corners or ceiling edges. Such improvements will form the basis for an elaborate architectural exploration of *RPS*. However, to fully control the fabrication parameters to transition to the existing building structure, a further investigation is necessary in the next steps of the research.

**Application to building structure, data collection, prediction and visualization informing the design process prior to fabrication** During the course of the 1:1 scale application, 32 segments were sprayed, which resulted in a large set of data collected. In addition to the linear model used in the presented work, within the research of *RPS*, the goal is to predict and visualize the effect of the fabrication parameters in line with the material, also with nonlinear functional relations. Therefore, the collected data will be used to train the

nonlinear regression model described in [5]. This approach enables an empirical but unique and intuitive understanding of a complex material process for the user, which would be possible through years of training and experience. However, the *Intel RealSense Depth Camera D455* used, limits the output of the data sets to a rough estimate of sprayed plaster thickness and as a result, to overall geometry or pattern, lacking details on diverse textures and thus lacking an assessment of the accuracy of the prediction (Figs. 6 and 9). It is used as an approximate visual representation to inform the design process. As a next step, the sensing system will be extended (with a high-accuracy time-of-flight camera) to allow for data collection on the quality of the sprayed results. This enhancement will allow us to explore higher resolution meshes for data collection, as exemplified in Fig. 10. Thus, the research will be able to address more of surface roughness and textures in addition to the overall volumetric geometry by developing a more accurate prediction model to inform the design process. Additionally, an extended sensing system can be benchmarked with other scanning systems and an assessment of the accuracy could be enabled, thus the assessment of the deviations between the intended geometry, pattern or quality and the as-built state could be done.

## Outlook

The application presented in this paper and the explorations in the previous studies have shown a great potential for *RPS* to offer a re-interpretation of the production of bespoke, cementitious plasterwork. To allow the designers to have an intuitive access to its possibilities, a catalogue of different geometries, patterns and volumetric formations is being continuously developed, within the *RPS* research, in relation to material properties. The research on *RPS* also aims to further investigate how to transfer the methods to other materials used for plasterwork, such as clay or gypsum, as well as to high-performance insulation and acoustic plasters, which often come with special application requirements in terms of thickness and geometry. Moreover, the robotic process can be extended to explore different techniques used

in manual plastering, such as rubbing, combing or stamping, and their effect on the surface geometry and texture. Thus, the goal is to revisit the typical functions of plaster as providing durability, insulation and weather protection to the building structure while also seeking to understand how the material and its geometric complexity can provide visual, acoustic or light diffusing effects. For this, as a starting point, the performative aspects of these geometries, patterns and formations are being investigated to understand the interdependence of different process parameters. This research can eventually allow us to better explore how the functional layers of the building structure can be combined with the ornamental qualities of the material through the dynamic forming of the wet material directly on the building structure.

*RPS* has the potential to be used in many applications, including in the design and fabrication of interior plaster-work on walls and ceilings as well as on facades and in the repair or reconstruction of existing structures. The novelty of *RPS* lies in the proposed gravity resisting, non-horizontal printing technique and in the strong relation between the material behavior and the geometric control during fabrication. The inherent capability of this technique to adapt dynamically to the as-built state of the on-going fabrication or the existing building structure and the methods developed have the potential to be transferred to other spray-based 3d-printing techniques for construction with cementitious or non-cementitious materials.

**Acknowledgements** This research was partially supported by the Swiss National Science Foundation (NCCR Digital Fabrication Agreement no. 51NF40-141853) and by the HILTI group. The authors acknowledge the students of the the MAS ETH in Architecture and Digital Fabrication program, Evgenia Angelaki, Liya Sunny Anthraper, Pascal Bach, Yen-Fen Chan, Wei-Ting Chen, Wei Chengyuan, Ilaria Giacomini, Simon Griffioen, Guillaume Jami, Eleni Kitani, Artemis Maneka, Beril Önalan, Foteini Salveridou, Priyank Soni, Ko Tsuruta, Carlos Wilkening. The authors would like to thank Valens Frangez for providing the sample scan data collected with the time-of-flight camera. Philippe Fleischmann, Andreas Reusser, Tobias Hartmann, and Michael Lyrenmann are acknowledged for their technical support. Eberhard Unternehmungen and Giovanni Russo AG are acknowledged for their logistic and technical support and sponsorship.

**Funding** Open access funding provided by Swiss Federal Institute of Technology Zurich

## Declarations

**Declarations** On behalf of all authors, the corresponding author states that there is no conflict of interest.

**Open Access** This article is licensed under a Creative Commons Attribution 4.0 International License, which permits use, sharing, adaptation, distribution and reproduction in any medium or format, as long as you give appropriate credit to the original author(s) and the source, provide a link to the Creative Commons licence, and indicate if changes were made.

The images or other third party material in this article are included in the article's Creative Commons licence, unless indicated otherwise in a credit line to the material. If material is not included in the article's Creative Commons licence and your intended use is not permitted by statutory regulation or exceeds the permitted use, you will need to obtain permission directly from the copyright holder. To view a copy of this licence, visit <http://creativecommons.org/licenses/by/4.0/>.

## References

- Göhler H, Gönül P, Spiro A (2012) Über Putz Oberflächen Entwickeln und Realisieren. gta Verlag, Zürich
- Millar W, Bankart GP, Orton J (2009) Plastering Plain and Decorative, 4th ed., reprinted by william millar and george p. bankart ; with an introd. by jeff orton ... [et al.] edn. Donhead, Shaftesbury (2009)
- Bard JD, Blackwood D, Sekhar N, Smith B (2016) Reality is interface: Two motion capture case studies of human-machine collaboration in high-skill domains. *Int J Archit Comput* 14(4):398–408. <https://doi.org/10.1177/1478077116670747>
- Bard J, Cupkova D, Washburn NR, Zeglin G (2018) Robotic concrete surface finishing: a moldless approach to creating thermally tuned surface geometry for architectural building components using profile-3d-printing. *Construction Robotics* 2:53–65. <https://doi.org/10.1007/s41693-018-0014-x>
- Ercan Jenny S, Lloret-Fritschi E, Jenny D, Sounigo E, Tsai P-H, Gramazio F, Kohler M (2021) Robotic plaster spraying: Crafting surfaces with adaptive thin-layer printing. *3D Printing and Additive Manufacturing*. <https://doi.org/10.1089/3dp.2020.0355>
- Mitterberger D, Ercan Jenny S, Vasey L, Lloret-Fritschi E, Aeijmelaeus-Lindström P, Gramazio F, Kohler M (forthcoming) Interactive robotic plastering: Augmented interactive design and fabrication for on-site robotic plastering. <https://doi.org/10.1145/3491102.3501842>
- Ercan S, Meier S, Gramazio F, Kohler M (2019) Automated localization of a mobile construction robot with an external measurement device. In: Al-Hussein M (ed.) *Proceedings of the 36th International Symposium on Automation and Robotics in Construction (ISARC)*, pp. 929–936. International Association for Automation and Robotics in Construction (IAARC), Banff, Canada. <https://doi.org/10.22260/ISARC2019/0124>
- Ercan S, Lloret Fritschi E, Gramazio F, Kohler M (2020) Crafting plaster through continuous mobile robotic fabrication on-site. *Construction Robotics* 4, 261–271. <https://doi.org/10.3929/ethz-b-000455153>
- Rosenfeld Y, Warszawski A, Zajicek U (1993) Full-scale building with interior finishing robot. *Autom Constr* 2(3):229–240. [https://doi.org/10.1016/0926-5805\(93\)90043-W](https://doi.org/10.1016/0926-5805(93)90043-W)
- Forsberg J, Graff D (1995) Åke Wernersson: An autonomous plastering robot for walls and ceilings. *IFAC Proceedings Volumes* 28(11):301–306. [https://doi.org/10.1016/S1474-6670\(17\)46989-8](https://doi.org/10.1016/S1474-6670(17)46989-8). 2nd IFAC Conference on Intelligent Autonomous Vehicles 1995, Espoo, Finland, 12–14 June 1995
- Pritschow G, Kurz J, Zeiher J, McCormac SE, Dalacker M (1997) On-site mobile plastering robot: A practical design concept. In: Whittaker W, Osborn J (eds.) *Proceedings of the 14th IAARC/IFAC/IEEE International Symposium on Automation and Robotics in Construction*, pp. 277–285. International Association for Automation and Robotics in Construction (IAARC), Pittsburgh, PA, USA. <https://doi.org/10.22260/ISARC1997/0034>
- Bock T, Buzalo N, Bulgakov A (2018) Mathematical description and optimization of robot control for plastering works. In: 2018 International Multi-Conference on Industrial Engineering and Modern Technologies (FarEastCon), pp. 1–5 . <https://doi.org/10.1109/FarEastCon.2018.8602717>

13. OKIBO (2021) The autonomous wall plastering robot. Accessed online 18.10.2021. <https://okibo.com/>
14. Bard J, Gannon M, Jacobson-Weaver Z, Jeffers M, Smith B, Contreras M (2014) Seeing is doing: Synthetic tools for robotically augmented fabrication in high-skill domains. In: 34th Annual Conference of the Association for Computer Aided Design in Architecture (ACADIA), pp. 409–416
15. Frangez V, Salido-Monzú D, Wieser A (2021) Surface finish classification using depth camera data. *Autom Constr* 129:103799. <https://doi.org/10.1016/j.autcon.2021.103799>
16. Özcan B, Schwermann R, Blankenbach J (2021) A novel camera-based measurement system for roughness determination of concrete surfaces. *Materials* 14(1). <https://doi.org/10.3390/ma14010158>
17. Bard J, Bidgoli A, Chi WW (2019) Image classification for robotic plastering with convolutional neural network. In: Willmann J., Block P, Hutter M, Byrne K, Schork T (eds.) Robotic Fabrication in Architecture, Art and Design 2018, pp. 3–15. Springer, Cham. [https://doi.org/10.1007/978-3-319-92294-2\\_1](https://doi.org/10.1007/978-3-319-92294-2_1)
18. Lindemann H, Gerbers R, Ibrahim S, Dietrich F, Herrmann E, Dröder K, Raatz A, Kloft H (2019) Development of a shotcrete 3d-printing (sc3dp) technology for additive manufacturing of reinforced freeform concrete structures. In: Wangler T, Flatt RJ (eds.) First RILEM International Conference on Concrete and Digital Fabrication – Digital Concrete 2018, pp 287–298. Springer, Cham. [https://doi.org/10.1007/978-3-319-99519-9\\_27](https://doi.org/10.1007/978-3-319-99519-9_27)
19. Buswell R, Kinnell P, Xu J, Hack N, Kloft H, Maboudi M, Gerke M, Massin P, Grasser G, Wolfs R, Bos F (2020) Inspection methods for 3d concrete printing. In: Bos FP, Lucas SS, Wolfs RJM, Salet TAM (eds.) Second RILEM International Conference on Concrete and Digital Fabrication, pp 790–803. Springer, Cham. [https://doi.org/10.1007/978-3-030-49916-7\\_78](https://doi.org/10.1007/978-3-030-49916-7_78)
20. Taha N, Walzer AN, Ruangjun J, Bürgin T, Dörfler K, Lloret-Fritsch E, Gramazio F, Kohler M (2019) Robotic aerocrete - a novel robotic spraying and surface treatment technology for the production of slender reinforced concrete elements. In: Sousa JP, Xavier JP, Castro Henriques G (eds) Architecture in the Age of the 4th Industrial Revolution - Proceedings of the 37th eCAADe and 23rd SIGraDi Conference, vol 3, pp 245–254. CumInCAD, Ljubljana. <https://doi.org/10.3929/ethz-b-000387276>. 37th eCAADe + SIGraDi Conference: Architecture in the Age of the 4th Industrial Revolution (2019); Conference Location: Porto, Portugal; Conference Date: September 11-13, 2019
21. Frangez V, Lloret Fritsch E, Taha N, Gramazio F, Kohler M, Wieser A (2021) Depth-camera-based rebar detection and digital reconstruction for robotic concrete spraying. *Construction Robotics* 279. <https://doi.org/10.3929/ethz-b-000510949>
22. Vukorep I, Zimmermann G, Sablotny T (2020) Robot-controlled fabrication of sprayed concrete elements as a cyber-physical-system. In: Bos FP, Lucas SS, Wolfs RJM, Salet TAM (eds.) Second RILEM International Conference on Concrete and Digital Fabrication, pp 967–977. Springer, Cham (2020). [https://doi.org/10.1007/978-3-030-49916-7\\_94](https://doi.org/10.1007/978-3-030-49916-7_94)
23. Lu B, Li M, Wong TN, Qian S (2021) Effect of printing parameters on material distribution in spray-based 3d concrete printing (s-3dcp). *Autom Constr* 124:103570. <https://doi.org/10.1016/j.autcon.2021.103570>
24. Crick C, Jay G, Osentoski S, Pitzer B, Jenkins OC (2017) In: Christensen HI, Khatib O (eds.) Rosbridge: ROS for Non-ROS Users, pp. 493–504. Springer, Cham (2017). [https://doi.org/10.1007/978-3-319-29363-9\\_28](https://doi.org/10.1007/978-3-319-29363-9_28)
25. Pankert J, Hutter M (2020) Perceptive model predictive control for continuous mobile manipulation. *IEEE Robot Autom Lett* 5(4):6177–6184. <https://doi.org/10.3929/ethz-b-000426821>
26. Ercan Jenny S, Blum H, Gawel A, Siegwart R, Gramazio F, Kohler M (2020) Online synchronization of building model for on-site mobile robotic construction. In: Osumi FHTK Hisashi (ed.) Proceedings of the 37th International Symposium on Automation and Robotics in Construction (ISARC), pp. 1508–1514. International Association for Automation and Robotics in Construction (IAARC), Kitakyushu, Japan. <https://doi.org/10.22260/ISARC2020/0209>